Drone-Aided Electrical Current Sensing – A Breakthrough for Smart Grids

Khaled Osmani*, Detlef Schulz
Department of Electrical Engineering
Helmut Schmidt University/University of the Federal Armed Forces
Hamburg, Germany
*alosmani.k@hsu-hh.de

***Abstract* – This paper serves as an overview of the current progress concerning the DNeD (Digitalized, legally safe and low-emission airborNe inspection and grid data acquisition using automated Drones) project. DNeD aims to provide a full solution of an intelligent current sensor, integrable inside a dedicated drone-embedded sensor box. The research began with a brief survey of non-invasive current sensing technologies as a guide for the selection of the optimum current sensing physics. Afterwards, an all-optical sensor (MICATU RG235) was tested under laboratory conditions. The results from these tests were systematically tabulated. Concurrently, a study on magnetic field-based current sensing was performed using Finite Element Analysis (FEA) in COMSOL. This dual approach allows for a comprehensive evaluation of different sensing technologies. Ultimately, the study concludes that magnetic-based sensing, utilizing Hall effect sensors (e.g. DRV5055), is by far the most suitable approach. Additionally, the design of the sensor-box housing considered crucial mechanical factors such as robustness and weight. The design process utilized CAD models developed in SolidWorks, which form the backbone for real sensor-box manufacturing. Overall, the circuitry suggestions consisted of the development of analogue modulation electronic circuits, incorporating low pass filters, voltage dividers, and additional protective circuitry to ensure the reliability and accuracy of the sensor data. A prototype was developed, featuring Bluetooth as the communication protocol between the sensor-box and a remote system running MATLAB. Preliminary results indicate that the prototype effectively transfers dummy analogue voltage signals over distances up to 30 metres, demonstrating the feasibility of the design for practical applications. This comprehensive study not only addresses the mechanical and physical design aspects of embedding an intelligent sensor in a drone but also explores various current sensing technologies and their practical implementation. The findings provide a robust framework for future development and optimization of intelligent sensor systems in aerial applications.**

Keywords – Drones, intelligent sensors, smart grids, remote surveillance

NOMENCLATURE

CAD	Computer Aided Design
DNeD	Digitalized, legally safe and low-emission airborNe inspection and grid data acquisition using automated Drones
FEA	Finite element analysis
MFs	Magnetic Fields
TL	Transmission line

I. INTRODUCTION

The increasing demand for electrical energy necessitates a more flexible and robust electric grid to meet the evolving power requirements. The load demands of the grids are nowadays governed by new technological sectors such as electric mobility: the rise of electric vehicles and their continuous and systematic need for recharging creates a significant new load on the grid. Higher energy consumption is additionally manifested by the electrification of industrial processes as industries experience a transition from fossil fuel-based to electric power systems. The substantial amounts of power for data centres and cloud computing also contribute to the amplification of electric demands. Moreover, the increased adoption of electric cooling/heating systems in residential and commercial areas contributes to the increased power demand as well. As a result, critical challenges for power infrastructures are created. One significant obstacle is the excessive electrical load demand, straining the capacity of the existing grids. In other terms, electrical grids are pushed closer to their full potential. Such a strain leads to the burnout of electrical transmission networks as they are forced to full-capacity operation more frequently. Hence, the likelihood of failures is augmented due to the accelerated wear and tear resulting from the constant high demands. With these new challenges, conventional electric grids have become less reliable and more prone to breakdowns and frequent blackouts. Furthermore, resultant voltage sags and swells with their destructive effects on loads lead to further economic costs and inefficiencies. The new trend of smart grids is partially induced by such consequences. In the light of the escalating demands, there is a need to modernize and add intelligence to conventional electrical grids to ensure a stable and reliable power supply. Hence, smart grids can achieve better load management, real-time monitoring, and better reactions to prevent power disruptions. The digitalization of grids allows for a dynamic response towards modern energy consumption.

There are strategies for the transition to smart grids that aim to achieve this goal: smart energy meters, distribution automation, and microgrids [1]. On the one hand, smart meters provide real-time data, allowing thus for better energy consumption monitoring and energy costs savings. Additionally, smart meters enable two-way communications which improves load balancing and reduces downtime from outages. The disadvantages of smart meters are their high cost of installation, their need for extra infrastructure, and data privacy threats. Distribution automation on the other hand, ameliorates conventional grids by automating faults detection and service

restoration but requires a significant initial investment in infrastructure (e.g. sensors implementation, control systems, skilled labour, etc.). From a different perspective, microgrids enhance the overall grid's resiliency by providing localized power generation and continuous critical loads supply during outages. In effect, microgrids reduce downtime and transmission losses due to decentralized power generation. Even so, microgrids are implemented with high complexities, along with their dependencies for additional control, monitoring equipment, and technical challenges in coordinating multiple interconnected systems [1]. By addressing the identified research gap in the race towards smart grids, the "Digitalized, legally safe and low-emission airborNe inspection and grid data acquisition using automated Drones (DNeD)" project aims to employ a drone as a messenger for an intelligent non-invasive electric sensor on overhead transmission lines. In other terms, a sensor-box, embedding an intelligent sensor consisting of a payload for a drone, can be deployed on transmission lines, allowing thus for a remote monitoring of electrical current passing through the transmission line (TL). Eventually, data about the TL, acquired by the deployed sensor box, can be dynamically processed and visualized by a human operator at any time. Therefore, the suggested DNeD project adds a digital trace over conventional analogue electric grids, enhancing the grids' operation and maintenance by:

- enabling remote monitoring of overhead TL by providing real-time data (e.g. instantaneous measured current),
- establishing a mathematical framework for predictive data maintenance as maintenance needs are anticipated with leveraged data analytics,
- facilitating predictive extrapolation of the grid's status so that human operators can better anticipate potential issues and plan pre-emptive actions accordingly,
- enhancing the overall grid's performance as fault occurrences are minimized, hence improving reliability and efficacity of electrical distribution.

The rest of this paper consists as follows: Section 2 presents a short overview about the physics of non-invasive current sensing. Section 3 outlines a laboratory test of MICATU RG235 with tabulated measurements outcomes. Section 4 highlights a Finite Element Analysis (FEA) of Magnetic Fields (MFs) radiated around electrical transmission lines with complex stranded geometries. Section 5 presents the Computer Aided Design (CAD) of the suggested sensor box. Section 6 showcases the first trials of the proposed hardware implementation of the DNeD sensor. Section 7 highlights the suggested future work and conclusions.

II. Physics of non-invasive current sensing

In conjunction with the DNeD project description, the intelligent current sensor should be non-invasive as it will never have any physical connection with the TL. Since the drone shall deploy the sensor box onto the TL, the embedded current sensor within is hence expected to captivate data of the electrical current flow in the TL, at a distance. The design should also take into consideration the limitations caused by the sensor box itself (i.e. produced MFs can be limited in front of the embedded sensor due to the physical barrier of the sensor box). With that being said, the surveyed physics for remote current sensing during the realization of the DNeD project are mainly classified as either magnetic or optical based. For magnetic based sensors, they utilize Ampere's circuital law, relying on the generated magnetic flux in the circuit: this law relates the MF around a closed loop, to the flowing current within, as expressed in the integral form of Formula (1).

$$\oint B \cdot dl = \mu_0 \iint j.dS = \mu_0 I \tag{1}$$

With $\oint B \cdot dl$ representing the line integral of the magnetic field B around a closed loop, μ_0 the free space permeability, j the current density, and I the total electric current passing through the loop [2]. With the proportionality of the MF around a conductor loop with respect to the current through the loop, electrical currents can be measured non-invasively. An example of MF-based sensors with the above-described physics can be tunnel magnetic junction, magneto-resistor with a differential Rogowski coil, three-axis MF vertical sensor array, hall effect sensors with coupling matrix, vertical MF sensors array based on air-core coils, and circular array of MF sensors. Alternatively, optical-based current sensing utilizes the Faraday Magneto-Optical effect: it describes the rotation of the light polarization's plane, when it passes through a magneto-optical material, under the influence of an active MF. In other terms, the rotation angle of the polarized light is proportional to the strength of the magnetic field and the length of the material through which the light travels, as expressed in Formula (2).

$$\varphi = \mu \cdot V \cdot \int H\, dl \tag{2}$$

Such that μ , V represent the magneto-optical material's relative permeability and Verdet constant respectively, and H the magnetic field intensity generated by the measured current [2]. Accordingly, an applied current can be calculated (thus measured experimentally) indirectly after knowing its resulting magnetic field, which proportionally modifies the amount of the polarization's rotation. For the described optical physics an example consists of a fibre optic sensor with a polarization splitter and a Faraday rotator: incident light is divided into two polarization states, by means of the polarization beam splitter, where the final state of the polarization reflects the flowing current proportionally. The selection of the sensor's physics took into consideration key factors related to the actual sensor's power consumption, sensitivity, resolution, percentage of error, shape, size, etc. with a general comparative assessment as presented in Table 1.

Table I: Comparative assessment of magnetic and optical sensors.

	Sensor's physics	
	Optical	***Magnetic***
Pros	No flowing electrons	High sensitivity
	Dynamic current range	Ease of integration
	Fail-safe	Compact size
Cons	Susceptible to optical interference	Drift over time
	Limited historical data	Temperature sensitive
	Higher cost	Magnetic interference

Both physics of Table 1 share the remote ability for current sensing (i.e. without a direct contact with the conductor) hence their applicability in the DNeD project.

In regard to optical based sensors the considerations were taken with respect to their high immunity versus electromagnetic interference and accurate readings in environments with high electrical noise. Additionally, optical based sensors minimize the risk of fire-sparking with an enhanced safety against heat induced failures. Along with their fail-safe mechanism optical sensors sustain the safety of the sensor box. Therefore, it is decided to begin with an optical sensor as the data source of TL's electrical currents in the DNeD project.

III. MICATU RG235 LABORATORY TEST

As per previous recommendations, the all-optical RG235 sensor from MICATU, Inc. is tested in the high voltage laboratory of the Helmut Schmidt University/University of the Federal Armed Forces. The conducted tests to investigate its suitability of application inside the DNeD's sensor box began with a high-voltage setup. Forced voltage values ranged from 1.48 kV to 20.464 kV. Additionally, RG235 was subjected to different current values to be measured from 10 A to 60 A, as presented in the montage of Figure 1 [3].

Despite that at this stage of research no intention exists to involve voltage measurement in the DNeD's sensor, the work in [3] represented a general background for any future work. As can be seen from Figure 1, the SE-CUR-CLAMP-150-DC represents a current measurement reference, to record any error in measurement in a drone-emulated (i.e. subjection of the RG235 to systematic and repeated vibrations) environment. With the error estimation Formula (3), Table 2 represents the measurements outcome of the RG235.

$$\%\ Error = \frac{|(Reference\ value - measured\ value)|}{Reference\ value} \times 100 \qquad (3)$$

TABLE II: TABULATED VOLTAGE AND CURRENT MEASUREMENT DATA OF THE RG235 UNDER LABORATORY TESTS [3].

VOLTAGE MEASUREMENTS				
Ref. RMS voltage [kV]	Measured RMS voltage [kV] (no vibrations)	Measured RMS voltage [kV] (under vibrations)	Error [%] (no vibrations)	Error [%] (under vibrations)
1.542	1.530	1.500	0.77	2.72
2.573	2.563	2.646	0.39	2.84
3.762	3.719	3.851	1.14	2.37
5.199	5.228	5.026	0.56	3.33
6.385	6.469	6.553	1.32	2.63
7.946	7.969	8.161	0.29	2.71
8.641	8.692	8.414	0.59	2.63
9.875	10.035	10.129	1.62	2.57
10.318	10.241	10.596	0.75	2.69
12.847	13.049	12.516	1.57	2.58
14.726	14.920	14.965	1.32	1.62
16.203	16.273	16.058	0.43	0.89
18.912	19.120	18.611	1.10	1.59
19.624	19.996	19.419	1.90	1.04
CURRENT MEASUREMENTS				
Ref. RMS current[A]	Measured RMS current [A] (no vibrations)	Measured RMS current [A] (under vibrations)	Error [%] (no vibrations)	Error [%] (under vibrations)
10	10.11	9.71	0.89	2.90
20	20.31	20.77	1.55	3.84
30	30.62	31.01	2.07	3.37
40	40.46	41.31	1.14	3.28
50	49.66	52.12	0.68	4.24
60	60.15	60.88	0.25	0.18

A reliable performance with minimal interference risks was demonstrated by the RG235. This was mainly due to its fibre optical output. In addition, the RG235 supports internet

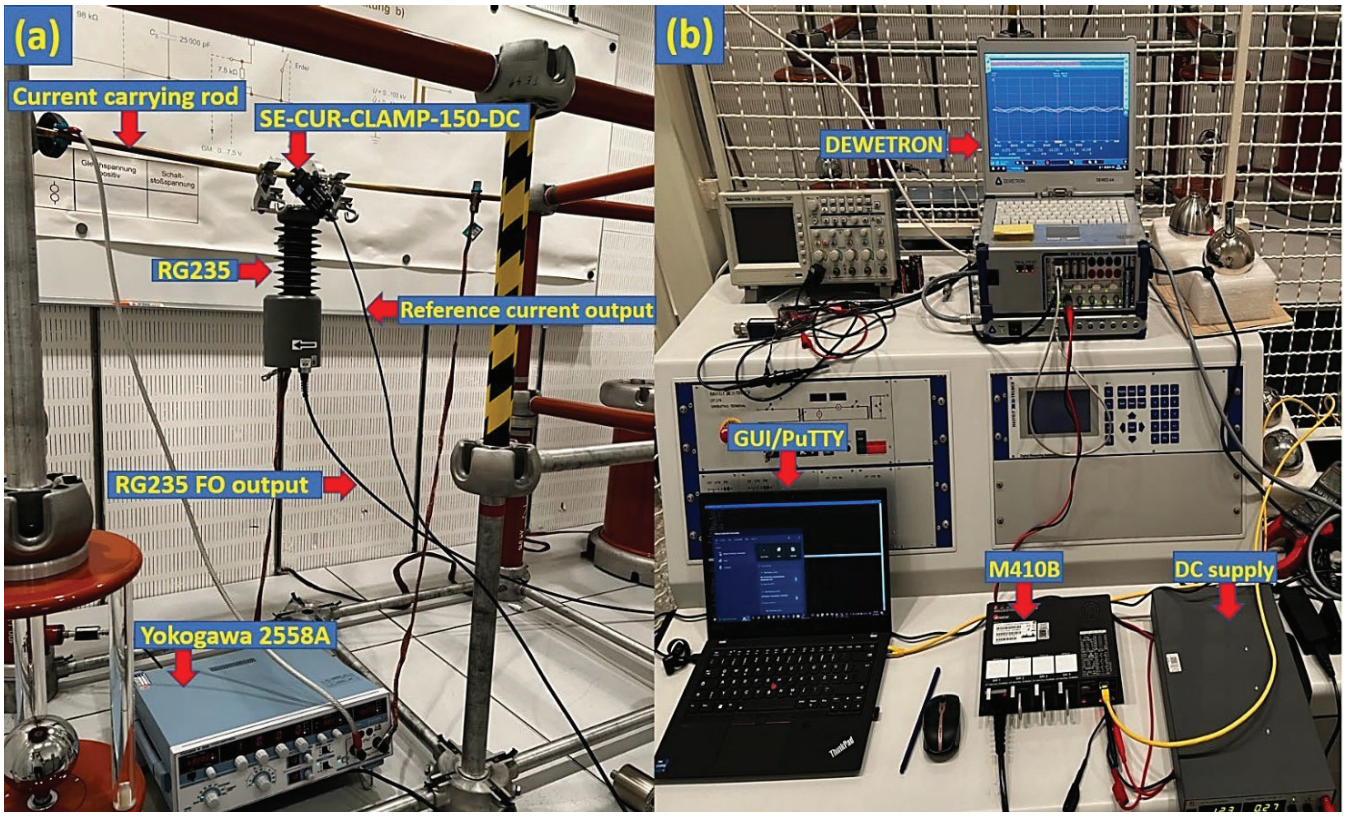

FIGURE 1: THE RG235 CURRENT MEASUREMENTS TEST SETUP: A) CIRCUITRY, B) OUTPUT ASSEMBLY [3].

protocol addressing enabling thus a dynamic remote access to the grid's operational status. Despite the safe and accurate measurements offered by the RG235, its bulky design limits its implementation in the DNeD's sensor box. Although it can be disassembled in a way that its internal Faraday's electro-optical current sensor is solely installed in the destined sensor box, that still poses fragility given the harsh working conditions of the DNeD project. At this point in the investigation, the idea to change the physics of the sensing technique had formed. Accordingly, the new approved sensing physics are magnetic based (i.e. done through magnetic based sensors such as hall effect or tunnel magnetoresistance).

IV. Finite Element Analysis (FEA) of MFs around complex stranded transmission lines in COMSOL

Based on the observations in [3], and in order to precisely select magnetic-based sensors, the study in [4] aimed for numerical data acquisition about current-induced MFs. In other words, the simulation in [4] guides the selection process of the magnetic based sensors' sensitivity. The geometric structure of overhead TLs (i.e. sub-filaments are redundantly stranded over each other) makes the MFs quantization around them hard to compute. Basically, for a single straight wire, the resulting MF due to current passage can be straightforwardly calculated with the numerical form of Biot-Savart law in Formula (4).

$$B = \frac{\mu_0 I}{2\pi R} \tag{4}$$

Such that μ_0 represents the free-space permeability, I the current, and R the distance from the wire to the point of observation [4]. This is not the case for stranded TLs: the stranded structure of overhead TLs, creates superimposing MF vectors of instantaneously varying norms/orientations. Therefore, it is hard to manually calculate the exact resulting MF around a stranded TL, at a specified point of observation in the space near the TL. For this reason, the Finite Element Analysis (FEA) in [4], executed by means of COMSOL Multiphysics 6.1 was conducted. It approximates as accurate as possible, the resulting MFs around stranded TLs, composed from 7-filaments (as shown in Figure 2) to 91-filaments. Table 3 encapsulates the resulting MFs norms after current injection from 10 A to 110 A in the 7-filament TL.

Table III: Resulting MFs due to the application of different current values in the 7-filament TL [4].

		$P(x;y;z)$			
Total current [A]	*Current in each filament*	*x [mm]*	*y [mm]*	*z [mm]*	*MF norm [mT]*
10	1.428	16	9	188	1.02×10^{-1}
		21	12	188	8.13×10^{-2}
20	2.857	13	9	188	2.37×10^{-1}
		19	13	188	1.65×10^{-1}
30	4.285	14	11	188	3.29×10^{-1}
		19	14	188	2.46×10^{-1}
40	5.714	14	9	188	4.76×10^{-1}
		18	16	188	3.24×10^{-1}
50	7.142	13	14	188	5.92×10^{-1}
		18	16	188	4.13×10^{-1}
60	8.571	15	9	188	6.65×10^{-1}
		18	15	188	5.05×10^{-1}
70	10	13	10	188	8.09×10^{-1}
		18	15	188	5.84×10^{-1}
80	11.428	14	9	188	9.32×10^{-1}
		17	15	188	6.78×10^{-1}
90	12.857	13	10	188	1.00
		19	14	188	7.40×10^{-1}
100	14.285	13	11	188	1.00
		17	16	188	8.32×10^{-1}
110	15.714	13	10	188	1.00
		16	16	188	9.28×10^{-1}

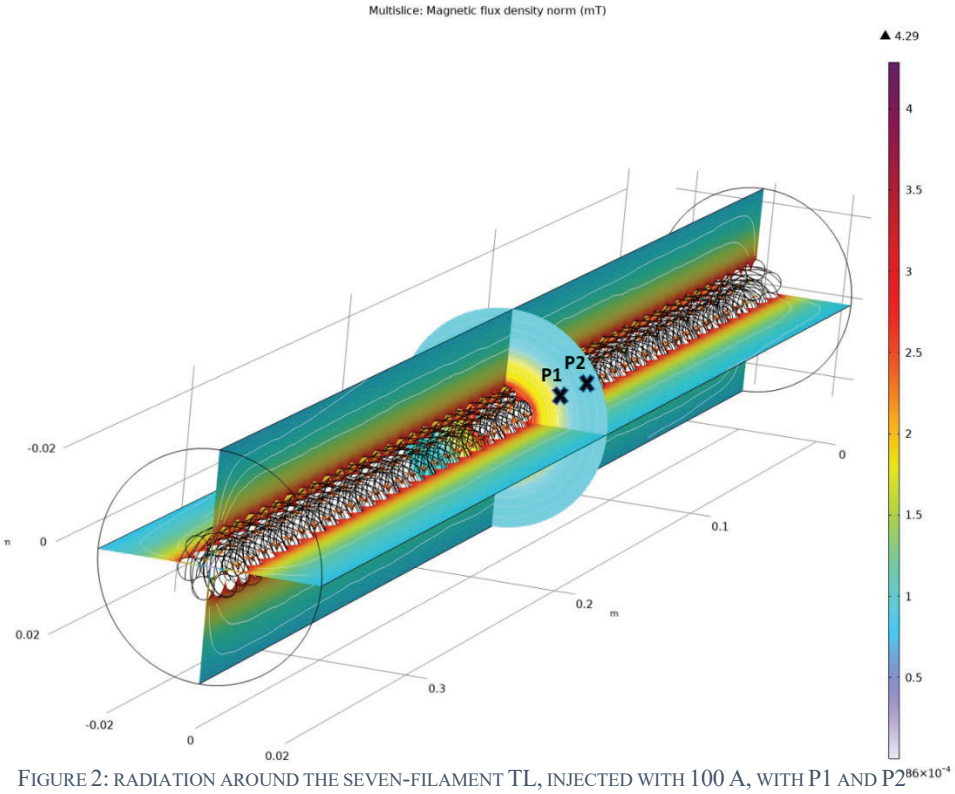

Figure 2: Radiation around the seven-filament TL, injected with 100 A, with P1 and P2$^{86\times10^{-4}}$ as the points of observation [4].

As an exemplary case of the 7-filament TL, the average resulting MF is valued at 5.74×10^{-1} mT. Accordingly, for this particular TL, with the two points of observation P1 and P2 as depicted in Figure 2, a magnetic based sensor with a [0 ; 1 mT] sensitivity range, should be able to detect MFs resulting from currents of 10 A to 110 A. Additionally, this study evaluated the MF sensors sensitivity ranges for larger currents (i.e. up to 1450 A in the 91-filament TL). In conclusion, the suggested MF based sensors can be designed for a large current range, which makes the application of the sensor box of Figure 3 more reliable.

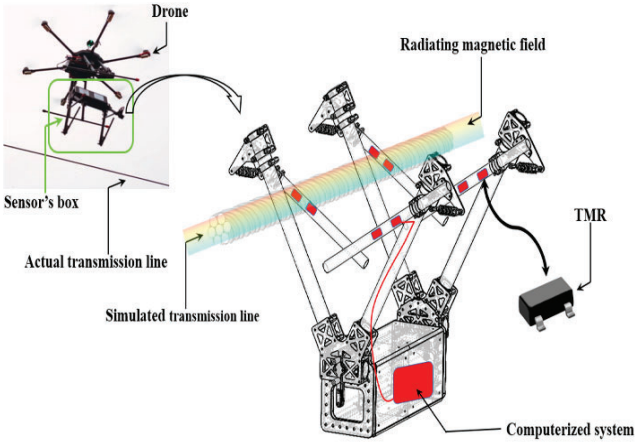

FIGURE 3: THE DNED'S PROJECT OVERVIEW [4].

V. SENSOR BOX CAD

With the recommended sensor workflow in [4], the sensor box should be manufactured based on certain design criteria to withstand various working conditions (e.g. environmental, operational integrity, etc.). With that being said, the sensor box should be lightweighted, robust, and non-magnetic. This is to avoid any interference with the MFs around the TLs. For these reasons, this part mainly accounts for the sensor box appropriate material and geometric design. Beginning with the sensor box material, it should have a high ingress protection to protect against water and dust penetration. Moreover, the sensor box should have a low magnetic permeability (Formula (5)) to allow the penetration of the MF into its internal space (where the MF sensor is installed) without any interactions.

$$\mu = \mu_0(1 + \chi_v) \tag{5}$$

Such that μ represents the magnetic permeability of the material, μ_0 the vacuum permeability, and χ_v the volume magnetic susceptibility [5]. Following the same perspective, the sensor box material must adhere to a robust structure. Since it is destined to be repeatedly laid onto/off the TL, it must present a high compressive strength, as approximated by the point on the engineering stress-strain curve $(\sigma_e^*, \varepsilon_e^*)$ defined in (6) and (7).

$$\sigma_e^* = F^*/A_0 \tag{6}$$

$$\varepsilon_e^* = l^* - l_0/l_0 \tag{7}$$

With σ_e^* representing the engineering stress, ε_e^* the engineering strain, F^* the load applied before the material's crashing, A_0 the material's original area, l^* the material's length before crashing, and l_0 the material's original length. Likewise, the optimum material should adapt to a high compressive strength (i.e. to withstand momentary axial loads without deforming/breaking) and a high tensile strength (i.e. ability to stay solid under pulling/stretching). Ultimately, in addition to a high ingress protection, low weight, high compressive/tensile strengths, the material should present high tensile modulus (i.e. rigidity) as represented in Formula (8).

$$E = \sigma/\varepsilon \tag{8}$$

With σ representing the compressive strength and ε the axial strength. By taking into account the mathematical model depicted by the Formulas (5)-(8), the chosen material for the sensor box construction is Carbon Fiber. From another side, the box' geometry must be easily integrable inside the drone. It should also attach securely to TL and resist environmental forces such as rain and wind. Subsequently, the designed sensor box consisted of a rectangular base and triangular fasteners, guaranteeing hence a stable attachment over the TL, and a secure fitting inside the drone as portrayed in Figure 4.

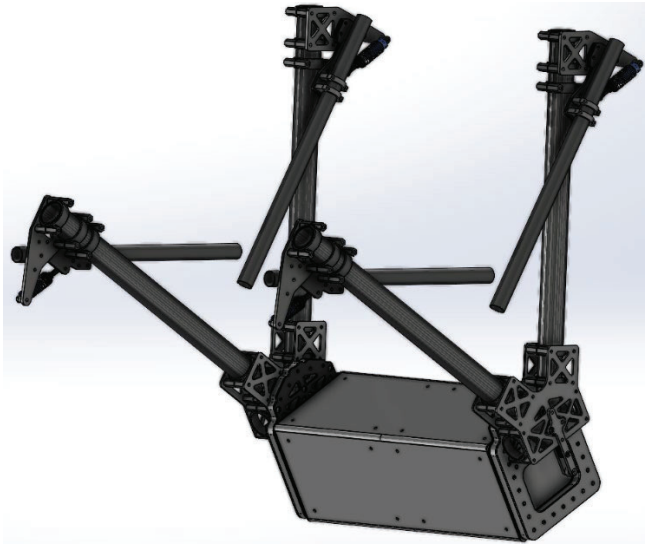

FIGURE 4: SENSOR BOX 3D FULL DESIGN WITH CARBON FIBRE AS CONSTRUCTING MATERIAL.

VI. FIRST TRIALS OF THE SUGGESTED HARDWARE

After the acknowledgement of the suggested current sensing physics (i.e. magnetic based), in addition to the recommended sensor box materials (i.e. carbon fibre) and geometry (i.e. Figure 4), the hands-on prototype realization can be started. First and foremost, initial tests can be manifested through a programmable DC voltage source as the source of information for flowing current, instead of applying a real MF sensor. Since an MF sensor would produce a voltage proportional to the sensed MF, the trial here is to only utilize dummy voltages to proceed with further tasks (e.g. communication, etc.). Such a DC voltage is to be processed via a small computerized system (e.g. Arduino Due), to be then processed wirelessly (i.e. via Bluetooth) to a MATLAB environment. This montage can be graphically expressed as in Figure 5. The variable DC voltage source instead of a real MF sensor (e.g. DRV5055) bypasses any electronic-based problems, mainly related to impedance and grounding. Therefore, the implementation began with code programming in the Arduino IDE as

FIGURE 5: BLOCK DIAGRAM REPRESENTATION OF THE DNED SENSOR FIRST-STEPS HARDWARE IMPLEMENTATION.

well as in MATLAB, to send/receive the sensed voltages with the corresponding analogue to digital conversions. The actual montage is hence composed of a real Arduino Due board, two Bluetooth modules (HC-05), a DC power supply, and variable DC voltages to be inputted onto the analogue inputs of the Arduino, as shown in Figure 6. From the receiver side (i.e. a computer with installed MATLAB), a Bluetooth range extender is needed to ensure a proper data transmission through longer distances (i.e. mimicking the distance between the sensor box installed on the overhead TL and the base station). The novelty behind codes implementation (instantaneous curve drawing of the sensed voltage norms), in both Arduino IDE as well as MATLAB, reflects the uniqueness behind the sensor workflow. The first trials revealed a successful data transfer between the test circuit (Figure (6, a)) and the receiver (Figure (6, b)), over a range of 30 metres.

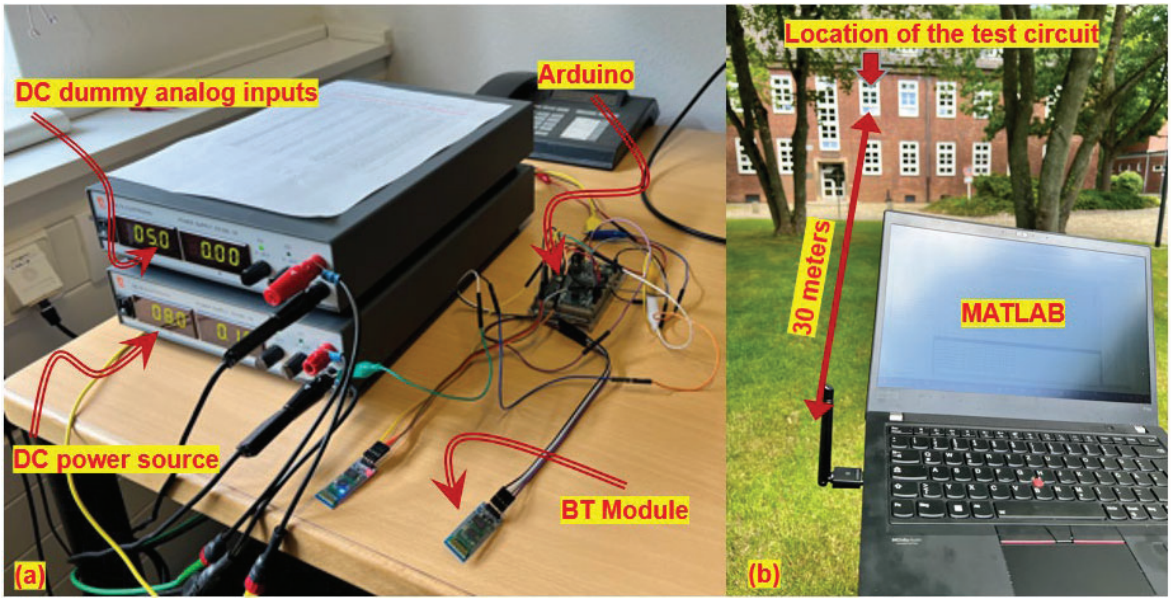

FIGURE 6: DNED'S PROTOTYPE FIRST TRIAL: A) TEST CIRCUIT, B) RECEIVER SIDE.

VII. CONCLUSION AND FUTURE WORK

The first outcomes of the test circuit with the receiver part showed encouraging results. The dummy voltages were able to be drawn instantaneously in MATLAB, over a distance of 30 metres with physical obstacles (e.g. wall, window). Next steps consist of implementing a real MF sensor such as the DRV5055 instead of the fixed DC supply, followed by filters and additional protection circuitry to ensure safe voltage values inputs at the Arduino analogue pins. The printed circuit board design shall be implemented inside the real Carbon Fiber sensor box to check how the range of 30 metres can be affected and react accordingly. Upon the full completion of the overall sensor design, a digital trace can be significantly added over TLs, allowing an actual sense of remote monitoring and analysis for electric grids.

ACKNOWLEDGEMENT

This research paper is part of the project DNeD ("Digitalisierte, rechtssichere und emissionsarme flugmobile Inspektion und Netzdatenerfassung mit automatisierten Drohnen", engl. "Digitalized, legally safe and low-emission airborNe inspection and grid data acquisition using automated Drones") and was funded by dtec.bw – Digitalization and Technology Research Centre of the Bundeswehr. dtec.bw is funded by the European Union – NextGenerationEU.

REFERENCES

[1] S. S. Mavuri, J. Nakka and A. Kotla, "Interconnected Microgrids: A Review and Future perspectives," 2022 IEEE 2nd International Conference on Sustainable Energy and Future Electric Transportation (SeFeT), Hyderabad, India, 2022, pp. 1-7, doi: 10.1109/SeFeT55524.2022.9908988.

[2] A. Ghasemi, "Chapter 1 – Fundamentals of ferrites", *Magnetic Ferrites and Related Nanocomposites, Micro and Nano Technologies*, 2022, pp. 301-367.

[3] K. Osmani, M. F. Meyer, F. Grumm and D. Schulz, "Toward Smarter Grids: Experimental Investigation of an "All-Optical" Electrical Sensor Under Laboratory Conditions," in *IEEE Access*, vol. 11, pp. 108418-108432, 2023, doi: 10.1109/ACCESS.2023.3321219.

[4] K. Osmani and D. Schulz, "Modeling Magnetic Fields around Stranded Electrical Transmission Lines via Finite Element Analysis (FEA)," *Energies*, vol. 17, no. 4, pp. 801–801, Feb. 2024, doi: https://doi.org/10.3390/en17040801.

[5] C. J. Bonin and F. J. Bonetto, "A Low-Cost and Accurate Method for Measuring Weak Magnetic Susceptibilities," in *IEEE Transactions on Instrumentation and Measurement*, vol. 71, pp. 1-10, 2022, Art no. 6002510, doi: 10.1109/TIM.2022.3165274.